JOURNAL OF APPLIED ELECTROCHEMISTRY 22 (1992) 204–214

Analysis of radiation-grafted membranes for fuel cell electrolytes

A. G. GUZMAN-GARCIA*, P. N. PINTAURO

Department of Chemical Engineering, Tulane University, New Orleans, LA 70118, USA

M. W. VERBRUGGE‡, E. W. SCHNEIDER§

‡*Physical Chemistry Department and* §*Analytical Chemistry Department, General Motors Research Laboratories, Warren, MI 48090-9055, USA*

Received 2 January 1991; revised 22 May 1991

One of the primary obstacles to be overcome for the development of economical fuel cells is the high cost of the membrane electrolyte. The currently favoured polymer electrolytes consist of poly(tetrafluoroethylene) backbone structures and poly(perfluorosulphonic acid) side chains. In an effort to find lower cost membranes, some radiation-grafted copolymer membranes were investigated. All the membranes contained poly(styrenesulphonic acid) side chains. Three different backbone polymer structures were studied: low-density poly(styrene), poly(tetrafluoroethylene)/poly(perfluoropropylene), and poly(tetrafluoroethylene). The results indicate that the membrane consisting of a poly(tetrafluoroethylene)/poly(styrenesulphonic acid) copolymer is a promising candidate as a fuel-cell electrolyte.

Nomenclature

A	transport channel cross-sectional area (cm^2)
N_A	Avogadro's number, 6.022×10^{-23} (mol^{-1})
c	concentration ($mol\,cm^{-3}$)
d	sample disc diameter (cm)
D	diffusion coefficient ($cm^2\,s^{-1}$)
F	Faraday's constant (96 487 C equiv.$^{-1}$)
i	current density ($mA\,cm^{-2}$)
k_Φ	electrokinetic permeability (cm^2)
$\mathscr{K}$	water exchange equilibrium constant
K	partition coefficient of the species ($c^{membrane}/c^{reservoir}$)
L	membrane thickness (cm)
m	membrane weight (mg)
n	number of mobile species
$\mathscr{N}$	number of radioactive atoms
N	molar flux ($mol\,s^{-1}\,cm^{-2}$)
P	pressure (atm)
$\mathscr{R}$	specific resistance ($\Omega\,cm^{-2}$)
R	universal gas constant ($8.314\,J\,mol^{-1}\,K^{-1}$)
S_0	specific surface (cm^2)
T	absolute temperature (K)
t	time (s)
t_j	transference number
v	pore-fluid velocity ($cm\,s^{-1}$)
V	membrane sample volume (cm^3)
x	distance (cm)
z	charge number

Greek symbols

δ	Kozeny-Carman pore breadth (nm)
θ	membrane porosity
κ	effective conductivity ($\Omega^{-1}\,cm^{-1}$)
λ	decay constant (min^{-1})
μ	fluid viscosity ($g\,cm^{-1}\,s^{-1}$)
ρ	density ($g\,cm^{-3}$)
σ	wall charge density ($C\,cm^{-2}$)
Φ	electric potential (V)

Subscripts

dry	conditions of dry membrane
H_2O	membrane equilibrated in pure water
j	ionic species
m	membrane
wet	conditions of wet membrane
*	radiotracer species

Superscripts

COLD	conditions in the cold reservoir
HOT	conditions in the hot reservoir
membrane	conditions inside the membrane
reservoir	conditions in the reservoir

1. Introduction

Over the last two decades, the need to develop high-efficiency power generators has been a major concern of the federal government [1], electric utilities companies [2], automobile makers [3–6], and other industrial concerns. A promising candidate is the fuel cell [7, 8], which is highly efficient, generates

* Now at Exxon Production Research Company, P.O. Box 2189, Houston, TX 77252-2189, USA.

0021-891X/92

relatively benign waste products and maintains quiet operation.

Ideally, a fuel cell converts the chemical energy of a fuel and an oxidant to electrical energy via a process involving essentially an invariant electrode–electrolyte system. In practice, however, corrosion of the structural materials, electrode-structure non-homogeneity, electrolyte degradation, and mass and heat transfer problems have slowed the development of the fuel cell as an economically competitive power source.

Two of the principal factors that limit long-term fuel cell performance are water management [9] and corrosion of cell components by the electrolyte [10]. In polymer-electrolyte fuel-cell systems, the electrolyte is confined to the pores of an ion-exchange membrane and corrosion effects are minimized. In these fuel cells, the membrane performance depends strongly on its water content; when fully saturated, the energy output from the fuel cell can be quite high as the membrane maintains a low ionic resistance.

In addition to corrosion and water management, it is necessary to consider the high cost of the electrodes and membrane materials. In general, polymer-electrolyte fuel cell electrodes that contain high platinum loadings produce high energy outputs. The commercially available membrane of choice for these high-energy-density cells is the perfluorosulphonic acid (PSA)* Nafion® 117 membrane [6, 11–13]. Using a Nafion-impregnated porous electrode, Ticianelli *et al.* [12] have been able to decrease the noble-metal loading while improving the level of performance of polymer-electrolyte fuel cells. Recently, Dow PSA membranes have shown an improved level of current density and power output in polymer-electrolyte fuel cells [14]. Since the PSA membrane is an expensive component of polymer-electrolyte fuel cells [13], it is important to identify promising, less-costly membranes and determine their transport characteristics.

Three membranes provided by RAI Research Corporation are analysed in this work using a series of radiotracer and electrochemical techniques which have been used previously by Verbrugge and Hill [17]. Experimental results are used to compute membrane conductivity, coion and water partition coefficients, coion and water diffusion coefficients, and membrane porosity. These results are combined with a macro-homogeneous transport mathematical model [16] to evaluate counterion diffusivity, membrane electrokinetic permeability, and an equivalent membrane-pore diameter. In the past, Nafion 117 [15, 16] and Dow PSA membranes [17] have been successfully characterized using similar techniques. Additional details about the approach can be found in [16] and [17]. The results of the present work are compared with the Nafion 117 and Dow membrane data.

* Nafion is a registered trademark of E. I. du Pont de Nemours and Company.

2. Experimental details

Samples provided by the RAIPORE Division of RAI Research Corporation included two fluorocarbon polymer matrix membranes (R-1010 and R-4010) and one hydrocarbon polymer matrix membrane (R-5010M). The first two digits in the product number identify the type of membrane matrix [18]:

R-*10*10 – TFE† Teflon

R-*40*10 – FEP‡/TFE Teflon

R-*50*10M – low density polyethylene

and the last two digits (. . . *10*) identify the ion-exchange membranes as *strong cationic*. The M in R-5010*M*, denotes *medium electrolytic resistance*. For all the membranes of this study, poly(styrene-sulphonate) pendant side chains provided the fixed charge groups. The thickness of each membrane in 0.6 N KCl and the ion exchange capacity of the dry membrane are: 0.045 mm and 1.2 meq g^{-1} for R-1010, 0.090 mm and 1.5 meq g^{-1} for R-4010, and 0.180 mm and 1.2 meq g^{-1} for R-5010M. In general, these membranes are much less expensive than Nafion 117 or other perflorosulphonic acid membranes [18]. The polymer backbone of Raipore membranes has been modified through the use of radiation grafting and cross-linking. Graft polymerization is known to produce thin membranes with good mechanical and electrochemical properties [19]. The experimental procedures and apparatus used to examine the equilibrium and transport properties of the membrane-electrolyte system are outlined in the remainder of this section.

2.1. *Membrane preparation*

Three discs of each membrane type were prepared by boiling each sample twice for 30 min in distilled water, then allowing the membranes to equilibrate at room temperature for at least 24 h in the sulphuric acid test solution.

2.2. *Membrane conductivity experiments*

The electrical resistance of the membrane samples was measured before and after exposing the membrane to an oxidizing medium. Prior to exposure to the oxidizing environment, resistance measurements were carried out with four different sulphuric acid concentrations: 0.3, 1.0, 3.0, and 5.0 M. For the oxidizing medium experiments, three discs of each membrane were boiled twice in distilled water and then allowed to equilibrate, at room temperature, in either 10% or 30% reagent-grade, stabilized hydrogen peroxide (J. T. Baker Chemical Company). After 2 days in the 10% H_2O_2 solution, or 13 days in the 30% H_2O_2 solution, the membranes were allowed to equilibrate

† TFE – tetrafluoroethylene

‡ FEP – a copolymer of tetrafluoroethylene and perfluoropropylene, also known as Teflon 100

in sulphuric acid for 24 h. Following the equilibration period, the membrane resistance was measured in 1.0 M sulphuric acid. These experiments allowed for a qualitative measurement of an oxidizing-medium effect on the membrane conductivity. The transport cell used for the membrane-resistance measurements can be represented as

Cold reservoir	*Membrane*	*Hot reservoir*
H^+	N^+	H^+
HSO_4^-	HSO_4^-	HSO_4^-
		$(^3H)OH$
		$H(^{35}S)O_4^-$
	$\longleftarrow \Delta\Phi \longrightarrow$	
	$\longleftarrow i$	
	$\longleftarrow v$	

A more complete drawing of the cell can be found in [16 or 17]. The voltage drop across the membrane is represented by $\Delta\Phi$, the current is given by i, and the pore fluid velocity is given by v. The cell consisted of two 100 mL Lucite reservoirs clamped together with the membrane separating the compartments. The transport channel had a cross-sectional area of 0.317 cm^2. At the platinum-screen electrodes the reactions are

$$\text{Anode: } 2H_2O \longrightarrow 4H^+ + O_2 + 4e^- \quad (1)$$

$$\text{Cathode: } 4H^+ + 4e^- \longrightarrow 2H_2 \quad (2)$$

Mercury/mercurous-sulphate reference electrodes were used to measure the potential drop across the membrane. Reagent-grade mercury (Merck) and mercurous sulphate (Allied Chemical) were used to construct the reference electrodes. After assembly of the cell, the acid electrolyte was added to each reservoir, and a current passed between the two platinum electrodes. To ensure that each reservoir concentration did not change significantly during an experiment, a square-wave, reversed-polarity, pulse current source was employed; the magnitude of the current was kept constant whereas its sign was reversed every 15 s. Currents of 8, 10, 12 and 14 mA (25.24, 31.54, 37.85, and 44.16 mA cm^{-2}) were applied. The current was controlled by an EG&G Princeton Applied Research model 273 potentiostat/galvanostat. A Nicolet 4094B digital, storage oscilloscope was used to record the potential difference between the reference electrodes. The data were stored on a floppy diskette for later analysis.

2.3. *Porosity experiments*

After the membrane discs were conditioned in the sulphuric acid test solution, they were blotted dry of excess surface solution, and the thickness and diameter were measured. The membranes were then boiled in distilled water and heated in a vacuum oven at 100° C for 6 h to remove absorbed water. The diameter and thickness of the membranes were measured once again. Discs of membrane R-1010 were weighed in the wet and dry states. Thicknesses were measured using a Starret 1010 constant-load dial gage, and diameters were measured by placing the membrane discs between glass slides and using a ruler. The dimensions from three discs at each acid concentration were averaged. Variations in the measurements were less than 6%. The porosity was computed from the membrane volume differences in the wet and dry states.

2.4. *Uptake analysis*

Three discs of each membrane type were equilibrated in a sulphuric acid solution of known concentration. After 24 h the discs were taken out of the solution, blotted dry to remove surface acid, and the thickness and diameter were measured. The three discs were then placed in a vial containing 10 mL of a sulphuric acid solution that was labelled with tritium (T) and sulphur-35 (^{35}S) (du Pont Research Products); the total acid concentration was the same as that used during the equilibration step. After 48 h, a 0.1 mL aliquot of the tagged acid solution was removed from the vial and injected into a counting vial containing 15 mL of liquid scintillation solution (Insta-Gel XF, Packard, Inc.) to determine the T and ^{35}S concentration in the solution. The membranes were withdrawn from the tagged solution, and one of two methods was used to remove surface electrolyte. In the first method, excess surface electrolyte was removed by quickly dipping the membranes containing the tagged species in distilled water. The second technique involved blotting the soaked membranes with filter paper to remove surface electrolyte. (Overall, the two techniques were comparable in accuracy and reproducibility.) The blotted (or rinsed) membranes were placed in a vial containing 15 mL of the liquid scintillation solution to determine the T and ^{35}S concentration in the membrane.

The radiotracer concentrations in the various samples were determined with a liquid scintillation spectrometer (Packard Tri-Carb 2200 CA), which incorporates a multichannel analyser to collect the energy spectrum of β-radioactivity. Measuring both T and ^{35}S concentrations simultaneously ensured that the same conditions exist for each species at the time of the measurement. The observed count rate for each species was converted to an absolute disintegration rate (disintegrations per minute or d.p.m.) by comparisons with separately prepared standards.

2.5. *Diffusion and electrodialysis experiments*

Self-diffusion experiments were carried out to obtain the diffusion coefficients of tritiated water and bisulphate ion. Electrodialysis experiments were conducted to measure the effect of applied currents on the flux of tritiated water. The apparatus for these experiments is similar to the cell schematic shown above. Each 50 mL reservoir contained a platinum electrode to allow for current passage across the membrane. A sampling port was used for the removal of electrolyte aliquots

during an experiment. The transport channel had a 0·785 cm^2 cross-sectional area. After assembly of the cell, a sulphuric acid solution was added to each reservoir; a radiotracer aliquot was then added to one of the compartments, henceforth referred to as the *hot* reservoir. (The chamber that originally contained no radiotracer will be referred to as the *cold* reservoir.) For these experiments, approximately 0.10 mL of a stock solution containing the T and ^{35}S radiotracers was added to 50 mL of electrolyte in the hot reservoir. The initial specific activity of this dual-label solution was 2.3 mCi mL^{-1} of T and 2.0 mCi mL^{-1} of ^{35}S (One curie (Ci) is the amount of radioactive material which decays at the rate of 3.7×10^{10} disintegrations per second [20]). Teflon-coated magnetic stirrers in each reservoir provided mixing of the electrolyte throughout an experiment.

Electrodialysis experiments were conducted first. The electrode in the hot compartment was made the anode. The electrochemical reactions at the platinum electrodes were identical to those in Equations 1 and 2. The starting time of these experiments was referenced to the introduction of radiotracer into the hot reservoir. Electrolyte aliquots of 10 μL were withdrawn from the hot compartment at the beginning and at the conclusion of each experiment to determine the upstream radionuclide concentration; 100 μL aliquots of electrolyte were withdrawn from the cold reservoir at five time intervals equally-spaced over the duration of the experiment. Glass micro-pipettes were used for the removal of radiotracer samples to ensure high accuracy in the determination of concentrations. The aliquots were added to 15 mL of scintillation solution for T and ^{35}S analysis. After delivery of the aliquot into the scintillation liquid, the micro-pipette was cleaned meticulously (with distilled water and acetone) to prevent contamination of the next aliquot. The duration of an electrodialysis experiment varied with the applied current; 75 min for 10 mA (12.7 mA cm^{-2}), 50 min for 100 mA (127 mA cm^{-2}), and 10 min for 400 mA (510 mA cm^{-2}). These times and currents were selected so that small, but approximately equal amounts of tritium were transported from the hot to the cold reservoir.

Dialysis experiments were carried out immediately after the three electrodialysis experiments. Each experiment lasted 2 h to ensure an accurate measurement of concentration changes in the cold-side chamber. Again, 100 μL aliquots of electrolyte were withdrawn from the cold reservoir at five time intervals equally-spaced over the duration of an experiment. The aliquots were added to 15 mL of scintillation solution for T and ^{35}S determination.

3. Results and discussion

3.1. *Membrane conductivity*

The electrical resistance of the different membranes was measured at different acid concentrations by applying square-wave, pulse currents and by measuring the potential difference between the two reference electrodes. During these polarization experiments, a pseudosteady-state was attained after 15 cycles. Plotted in Fig. 1 is a typical example of the applied square-wave current source (bottom graph) and the resulting potentials (top graph) for membrane sample R-1010 in 1.0 M H_2SO_4. The membrane sheet resistance ($\mathscr{R}_{sheet}$) was obtained by subtracting the cell resistance in the abscence of the membrane ($\mathscr{R}_{cell}$) from the cell resistance with the membrane present ($\mathscr{R}_{total}$)

$$\mathscr{R}_{sheet} = \mathscr{R}_{total} - \mathscr{R}_{cell} \tag{3}$$

The resistance is calculated from each polarization experiment by the relation

$$\mathscr{R} = \frac{\Delta\Phi}{i} \tag{4}$$

The resistances for all three membranes in the different sulphuric acid solutions are plotted in Fig. 2. The sheet resistance was lowest in the 1.0 M sulphuric acid solution. The thinnest membrane had the lowest sheet resistance for all acid concentrations. Since the membrane resistance is an important characteristic to consider for fuel-cell operation, the sheet resistance of the three radiation-grafted copolymers is compared to that of Nafion and the Dow polymers (reported by Verbrugge and Hill, [17]) in Fig. 3. Both R-1010 and R-4010 compare favourably with the du Pont and Dow membranes.

We define the effective membrane conductivity κ_{eff} as

$$i = -\kappa_{eff}\frac{d\Phi}{dx} \tag{5}$$

When $d\Phi/dx$ is approximated by $\Delta\Phi/L$, (where L is the membrane thickness), the membrane effective conductivity is given by

$$\kappa_{eff} = -\frac{iL}{\Delta\Phi} \tag{6}$$

The effective conductivity of the three membrane samples is shown in Fig. 4. For all three RAI membranes, the conductivity was highest in the 1.0 M sulphuric acid solution. It is interesting to note that this result was also observed with the Nafion and Dow polymers [17]. Polymer membranes exhibiting conductivities between 0.001 and 0.1 $\Omega^{-1}cm^{-1}$ at 25° C are of interest for fuel cell applications [22]. Based on the experimental conductivity data alone, all three RAI membranes may be of interest for use in fuel cells.

To estimate the effect of the oxidizing environment in a polymer-electrolyte fuel cell, the membrane samples were exposed to H_2O_2. A comparison of the conductivity before and after exposure to hydrogen peroxide is shown in Fig. 5 for the three RAI membrane samples. In the 10% H_2O_2 solution, the conductivity of membrane R-1010 decreased by only 15%; the conductivity of sample R-4010 decreased by two-orders of magnitude, and that of R-5010M by one-order of magnitude. The membrane

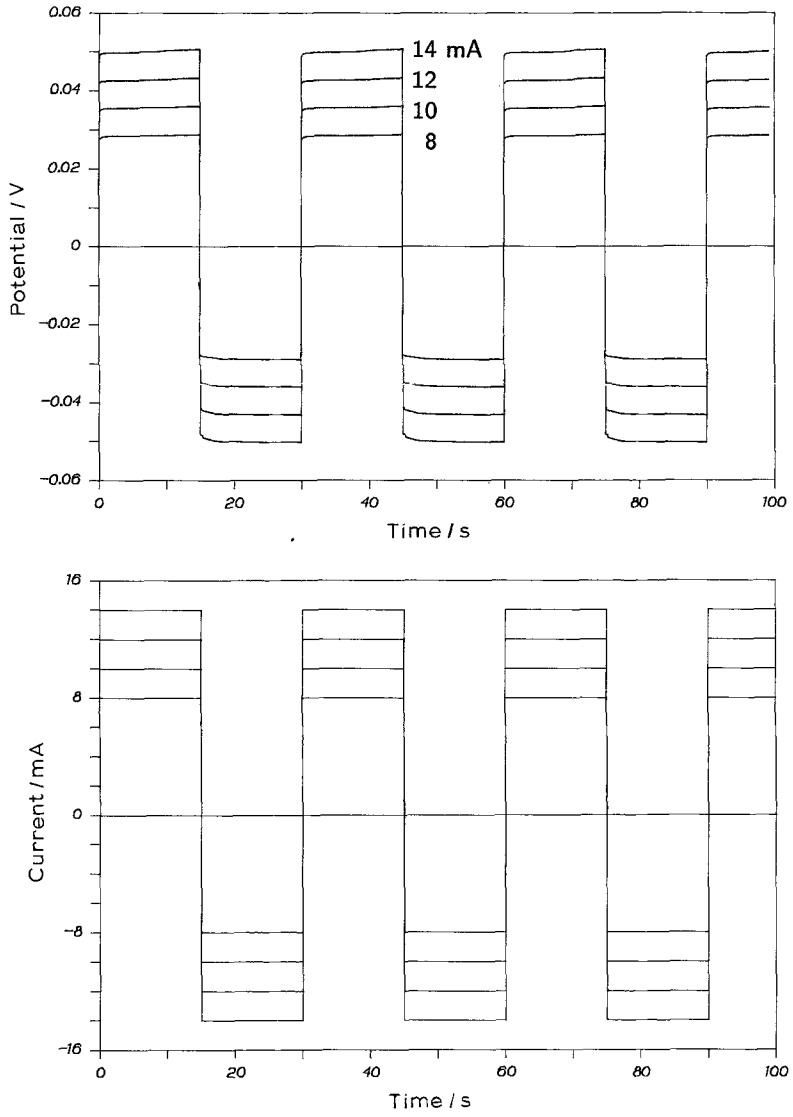

Fig. 1. Typical example of applied square-wave current source (bottom) and the resulting potentials (top) for membrane sample R-1010 in 1.0 M H_2SO_4.

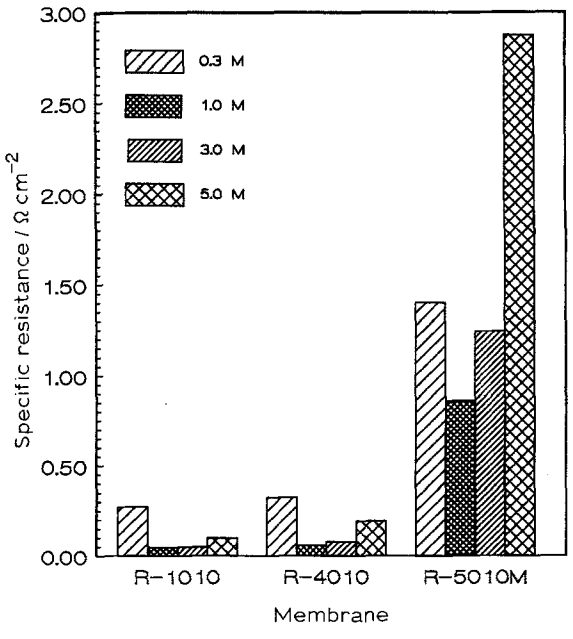

Fig. 2. Specific resistance for each membrane in different sulphuric acid solutions.

conductivity after soaking in 30% H_2O_2 decreased by at least five orders of magnitude for all three RAI samples. The results in Fig. 5 suggest that transport of ions across the membrane is severely hindered in the R-4010 and R-5010M membranes. The propensity of membranes R-4010 and R-5010M to degrade in an oxidizing environment diminishes their potential for use in fuel cells. Membrane sample R-1010, on the other hand, may be able to withstand a mild oxidizing environment while remaining highly conductive.

3.2. *Membrane porosity*

It is generally recognized that ion-exchange membranes, upon absorption of solute and solvent, will expand or swell. The membrane porosity is a measure of this volume increase. Cross-linked ion-exchange membranes also swell in water and polar solvents, but to a lesser degree due to the intricate linking of the polymer-chain backbones.

To calculate membrane porosities, the thickness L and diameter d of the R-4010 and R-5010M membrane

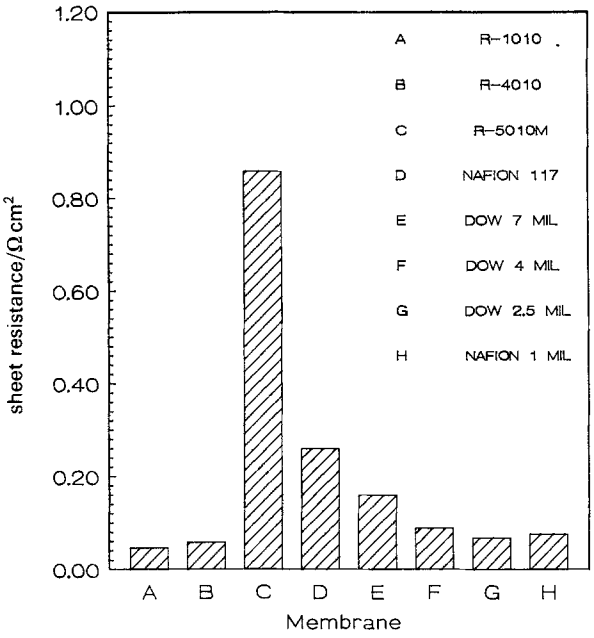

Fig. 3. Comparison of sheet resistance for the three radiation-grafted copolymers with Nafion and the Dow polymers.

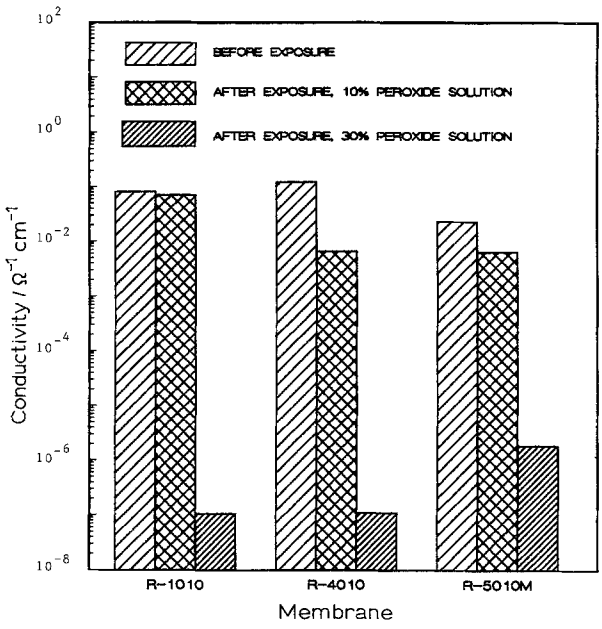

Fig. 5. Comparison of the conductivity before and after exposure to H_2O_2 for the three RAI membrane samples.

disks were measured in the dry and wet states. The membrane volume was calculated by

$$V = \frac{\pi}{4} d^2 L \tag{7}$$

The porosity θ of membranes R-4010 and R-5010M was determined from

$$\theta = \frac{V_{wet} - V_{dry}}{V_{wet}} \tag{8}$$

where V_{wet} is the volume of the membrane equilibrated in the acid solution of interest and V_{dry} is the dry membrane volume. The R-1010 membrane was the thinnest of the three samples. Its volume was difficult to measure and the following relationship was used to compute θ

$$\theta = \frac{\Delta V}{1 + \Delta V} \tag{9}$$

In Equation 9, ΔV is the volume increase of the membrane upon addition of an electrolytic solution per unit volume of dry membrane. ΔV is related to the experimentally measured wet and dry membrane weights (m_{wet} and m_{dry}, respectively) by

$$\Delta V = \frac{\rho_{dry}(m_{wet} - m_{dry})}{\rho_{acid} m_{dry} + \rho_{dry}(m_{wet} - m_{dry})} \tag{10}$$

where ρ_{dry} is the density of the dry membrane, and ρ_{acid} is the density of the external acid solution. Calculated porosities for the three membranes in different H_2SO_4 concentrations are listed in Table 1. For comparison, the porosity of Nafion 117 in sulphuric acid [15] solutions is also given.

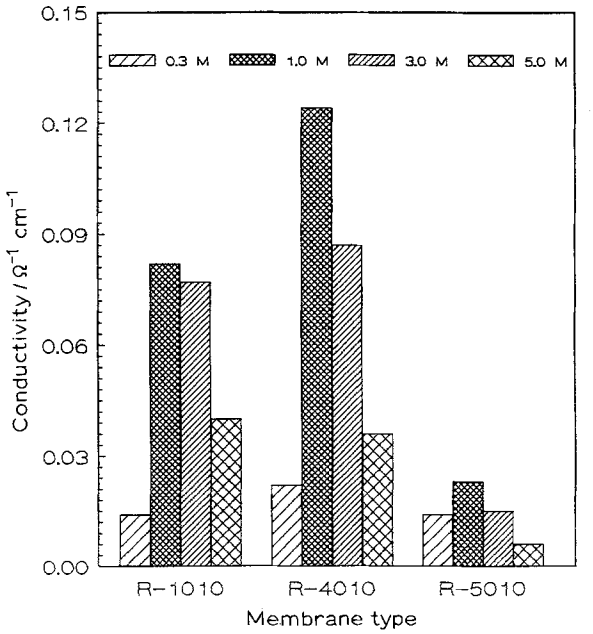

Fig. 4. Effective conductivity of the three membrane samples.

In the present study, the porosities of the membrane samples with the fluorocarbon polymer matrices (R-1010 and R-4010) were found to be larger than those of the hydrocarbon backbone (R-5010M) for all acid concentrations. The porosity generally decreased with increasing acid concentration in the range of 0.3 to 5.0 M. Membrane swelling depends on the solution concentration in contact with the membrane; membranes usually swell (increase in porosity) as the external electrolyte concentration is lowered [19]. Verbrugge and Hill [15] also observed a decrease in membrane porosity with increasing H_2SO_4 concentration in their work with Nafion 117. Likewise, Capeci *et al.* [24] reported decreasing porosities, from 0.25 to 0.18, for Nafion 110 with increasing NaCl concentration in the range of 1.0 to 5.0 M. The porosity of R-1010 at 5.0 M H_2SO_4, however, is larger than that in 3.0 M acid. We attribute this increase in membrane porosity to experimental errors. Membrane sample R-1010 was the thinnest of the three RAI membranes, and it was

Table 1. Effective membrane porosities of the three RAI membranes in different sulphuric acid concentrations incorporating the results reported in [15] for Nafion 117

Membrane	*0.3 M*	*1.0 M*	*3.0 M*	*5.0 M*
R-1010	0.37	0.33	0.30	0.38
R-4010	0.46	0.40	0.32	0.28
R5010M	0.26	0.22	0.14	0.15
Nafion 117	0.29	0.28	0.27	–

difficult to accurately measure the membrane volume and to adequately remove surface acid.

3.3. *Uptake analysis*

The distribution or partition coefficient (K) is defined as the ratio of the concentration of a species in the membrane to that in the external solution [19].

$$K_{\text{species}} = \frac{c_{\text{species}}^{\text{membrane}}}{c_{\text{species}}^{\text{reservoir}}} \tag{11}$$

The partition coefficients of acid and water ($K_{H_2SO_4}$ and K_{H_2O}) were determined in the present study from radiotracer absorption experiments. The number of radioactive atoms present in a membrane sample was determined by the relationship

$$\frac{d\mathcal{N}_j}{dt} = \lambda_j \mathcal{N}_j \tag{12}$$

where $d\mathcal{N}_j/dt$ is the disintegration rate of the radionuclide j in the membrane sample with units of d.p.m. (disintegrations per minute), λ_j is the radionuclide decay constant, and $\mathcal{N}_j$ is the number of radioactive atoms of species j. The decay constant λ_j is $1.07 \times 10^{-7}\,\text{min}^{-1}$ for T and $5.52 \times 10^{-6}\,\text{min}^{-1}$ for ^{35}S.

To calculate the water concentration within the membrane, the T count ($\mathcal{N}_T$) obtained from Equation 12 was used. In bulk water, the tritium species partitions into T^+ and THO according to the facile exchange reaction

$$H_2O + T^+ \rightleftharpoons THO + H^+ \tag{13}$$

(Note: there are two hydrogen atoms per water molecule and one tritium atom per THO molecule.)

The ratio of the tritiated species to the hydrogen species is

$$\frac{c_{T+}}{c_{THO}} = \frac{c_{H+}}{2c_{H_2O}} \tag{14}$$

Electroneutrality for the whole system must be satisfied; the total number of experimentally measured tritium species ($\mathcal{N}_T$) within the membrane is given by

$$\mathcal{N}_T = \mathcal{N}_{THO} + \mathcal{N}_{T+\ldots SO_3^-} + \mathcal{N}_{T+\ldots HSO_4^-} \tag{15}$$

The number of tritium ions associated with the fixed-charge sites ($\mathcal{N}_{T+\ldots SO_3^-}$) was determined from the membrane equivalent weight EW (grams of dry polymer per mol of sulphonic acid site), dry density

Table 2. Water partition coefficients for the three RAI membranes in different sulphuric acid concentrations. Water partition coefficients for Nafion 117 [15] and Dow membranes [17] in H_2SO_4 are also included

Membrane	*0.3 M*	*1.0 M*	*3.0 M*	*5.0 M*
R-1010	0.74	0.97	0.92	0.78
R-4010	0.26	0.25	0.30	0.33
R-5010M	0.72	0.73	0.64	0.50
Nafion 117	0.34	0.32	0.28	–
Dow 7-mil	–	0.39	–	–
Dow 4-mil	–	0.36	–	–
Dow 2.5-mil	–	0.34	–	–

ρ_{dry}, and dry volume V_{dry}

$$\mathcal{N}_{T+\ldots SO_3^-} = \frac{\rho_{dry} V_{dry} N_A}{EW} \tag{16}$$

where N_A is Avogadro's number. The number of tritium ions associated with the bisulphate anions ($\mathcal{N}_{T+\ldots HSO_4^-}$) was obtained directly from the ^{35}S counts. Equation 15 was solved for $\mathcal{N}_{THO}$, and the membrane water concentration was obtained from the THO/H_2O ratio specified in Equation 14. Water partition coefficients for the three membranes in different H_2SO_4 concentrations, together with those for Nafion 117 [15] and three Dow membranes [17] in 1.0 M H_2SO_4, are listed in Table 2. It should be noted that the water partition coefficients of R-1010 and R-5010M are much larger (by at least 87%) than those of the Nafion and Dow membranes in 1.0 M acid. Prior studies have shown that the membane water content decreases with increasing concentration of solute in the external solution [19]. This does not appear to be the case for the RAI membranes examined in this study. The water partition coefficients of membrane samples R-1010 and R-5010M go through a maximum at 1.0 M H_2SO_4 and then decreases with increasing external electrolyte concentration. Pintauro and Bennion [25] reported that the water partition coefficient for Nafion 110 and NaCl electrolytes decreased linearly with increasing salt concentration in the range of 1.0 and 5.0 M. Similarly, Verbrugge and Hill [15] in their sulphuric acid-Nafion 117 work, report decreasing water partition coefficients with increasing H_2SO_4 concentration between 0.3 and 10.0 M. The water partition coefficient for membrane R-4010 increases continuously with increasing H_2SO_4 concentration. No such trend has been reported in the literature for similar electrolyte-membrane systems.

It is often helpful to examine the coion adsorption and transport characteristics of membrane-electrolyte systems. The resulting selectivity data, for example, can be used to elucidate probable pore structures [24]. The results of coion partition coefficient experiments for the RAI membranes in different H_2SO_4 concentrations are listed in Table 3 along with the coion partition coefficients for H_2SO_4/Nafion 117 [15] and H_2SO_4/Dow membranes [17]. The bisulphate ion partition coefficient increases with external acid concentration for all membranes. This result is in agreement

Table 3. Bisulphate ion partition coefficients for the three RAI membranes in different sulphuric acid concentrations. Included also are the Nafion 117 [15] and Dow membranes [17] bisulphate ion partition coefficients

Membrane	*0.3 M*	*1.0 M*	*3.0 M*	*5.0 M*
R-1010	0.16	0.39	0.61	0.61
R-4010	0.07	0.10	0.43	0.60
R-5010M	0.13	0.22	0.29	0.28
Nafion 117	0.06	0.10	0.13	–
Dow 7-mil	–	0.12	–	–
Dow 4-mil	–	0.13	–	–
Dow 2.5-mil	–	0.15	–	–

with previous studies using Nafion 110 and aqueous NaCl (1.0–5.0 M), in which an increase in coion partition coefficient with increasing external electrolyte concentration was observed [25]. A qualitative explanation for this phenomenon is provided by the so-called Donnan potential which exists between the ion-exchange membrane and the bulk solution. The Donnan potential prevents the coion concentration within the membrane from rising beyond an equilibrium value which is usually much lower than the concentration in the external solution. The absolute value of the Donnan potential and the efficiency of electrolyte exclusion in an ion-exchange membrane decreases with increasing external concentration, thus lowering K [19].

3.4. *Diffusion experiments*

The diffusion coefficients of the bisulphate ion and water were determined from data collected in the dialysis experiments. The transfer of a radioactive isotope from the hot reservoir to the cold compartment in the absence of an applied current was recorded as the change in radiotracer concentration with time. The reservoir concentrations of each radiotracer species changes with time due to acid and water transport through the membrane. Variations in concentration are described mathematically by a material balance equation for the cold-side reservoir,

$$\frac{\partial c_*^{\mathrm{COLD}}}{\partial t} = N_* \frac{A}{V} \tag{17}$$

where c_*^{COLD} is the concentration of either THO or $H^{35}SO_4^-$ in the downstream reservoir, A is the membrane area, V is the reservoir volume, and N_* is the molar flux of tracer species. The tracer's molar flux can be described by Fick's First Law, and a linear concentration profile is obtained for the conditions of this work ($tD_*/L^2 \gg 1$, where D_* is the tracer diffusion coefficient corresponding to c_*, and L is the membrane thickness). For the tagged bisulphate ion $c^{\mathrm{HOT}}_{H^{35}SO_4^-} \gg c^{\mathrm{COLD}}_{H^{35}SO_{-4}}$ throughout an experiment, and the solution to Equation 17 is:

$$\frac{c^{\mathrm{COLD}}_{H^{35}SO_4^-}}{c^{\mathrm{HOT}}_{H^{35}SO_4^-}} = \frac{(D_{H^{35}SO_4^-})(K_{H^{35}SO_4^-})(A)}{LV} t \tag{18}$$

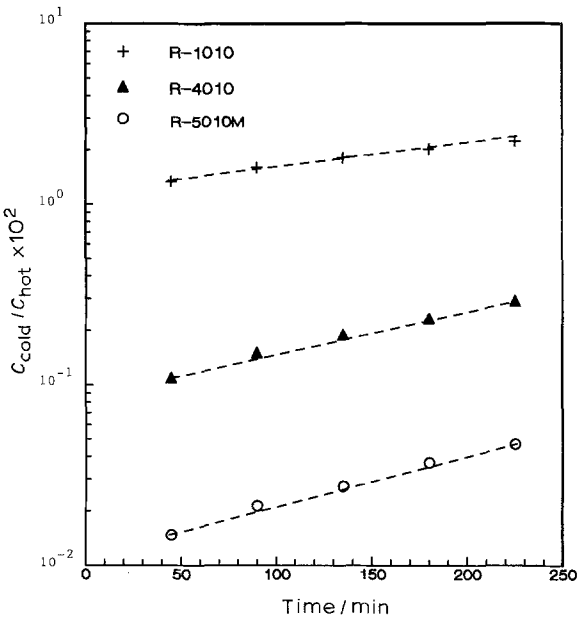

Fig. 6. Cold-side reservoir concentration of $H^{35}SO_4^-$ (normalized by the hot-side reservoir concentration) as a function of time for the three RAI membrane samples.

The experimentally determined cold-side reservoir concentration of $H^{35}SO_4^-$, normalized by the hot-side reservoir concentration, is plotted as a function of time in Fig. 6 for the three RAI membranes with 1.0 M H_2SO_4. By equating the slopes in this graph to $D_{H^{35}SO_4^-}K_{H^{35}SO_4^-}A/LV$, the diffusion coefficients of the bisulphate ion are calculated ($K_{H^{35}SO_4^-}$, A, L, and V are known constants).

At the beginning of the THO dialysis experiments there was a small amount of tritium in the cold-side reservoir since the electrodialysis experiments were conducted first. In addition, the hot side concentration changed significantly with time; integration of Equation 17 for this case yields:

$$\ln \frac{(c^{\mathrm{COLD}}_{\mathrm{THO}} - c^{\mathrm{HOT}}_{\mathrm{THO}})|_{\mathrm{initial}}}{c^{\mathrm{COLD}}_{\mathrm{THO}} - c^{\mathrm{HOT}}_{\mathrm{THO}}} = \frac{2K_{\mathrm{THO}}D_{\mathrm{THO}}A}{LV} t \tag{19}$$

Figure 7 presents linear plots of the logarithmic concentration of THO against time for the RAI membrane samples in 1.0 M H_2SO_4. The diffusion coefficient of the tritiated water species is calculated from the slope of any one line (K_{THO}, A, L, and V are known constants). The computed diffusion coefficients of water and bisulphate ion in 1.0 M H_2SO_4 for the three RAI membranes are listed in Table 4. Proton diffusion coefficients are also included in this table. D_{H^+} was determined from the electrodialysis experiments, as will be discussed in the following section. For comparison, diffusivities in Nafion and the Dow membranes are also listed in Table 4. Lower diffusion coefficients for water, bisulphate ions, and protons are obtained for the three RAI membranes as compared to those in Nafion and Dow membranes. This was expected because the degree of polymer cross-linking is higher in the radiation-grafted membranes. The bisulphate ion diffusion coefficient decreases due to electrostatic repulsion from the fixed-charge groups on the pore walls and from the tortuous diffusion

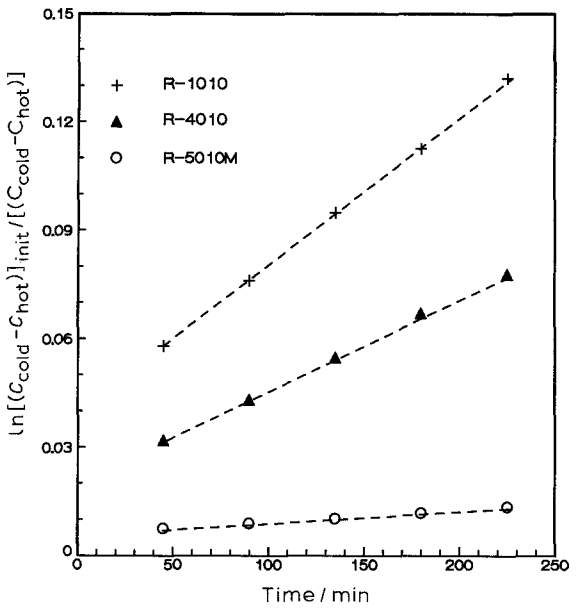

Fig. 7. Linear plots of the logarithmic concentration of THO against time for the three RAI membrane samples.

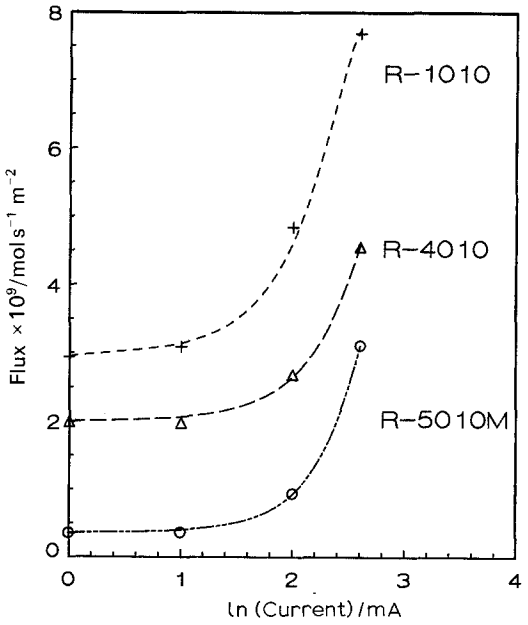

Fig. 8. Fluxes of titrated water during electrodialysis against current – model results.

path across the membrane. The reduction of the bisulphate ion diffusion coefficient is less pronounced than that of the proton for the radiation-grafted membranes, relative to the infinite-dilution values.

3.5. *Electrodialysis experiments*

The fluxes of tritiated water obtained during the electrodialysis experiments are plotted in Fig. 8. The electro-osmotic water flux in all the RAI membranes was found to increase with increasing current. Similar trends have been obtained for 1.0 M H_2SO_4 electrodialysis experiments with Nafion and Dow membranes [15, 16].

An analytical model previously employed for the Nafion/sulphuric acid membrane system [16] was used to compute the proton diffusion coefficient, the membrane electrokinetic permeability, and an equivalent pore diameter from the radiotracer electrodialysis experiments.

In an electrodialysis experiment, the system quickly reaches steady state, and time derivatives can be neglected. For this case, the species continuity and tritiated water flux equations can be combined to give

$$0 = D_{H_2O}\nabla^2 c_{THO} - v\nabla c_{THO} \qquad (20)$$

In this analysis it is assumed that the concentration of THO in the cold-side reservoir is zero, and the concentration in the hot-side reservoir remains constant throughout an experiment. Hence, the following boundary conditions apply:

$$c_{THO}(0) = 0 \qquad (21)$$

$$c_{THO}(L) = K_{H_2O}(c_{THO}^{HOT}) \qquad (22)$$

Equation 20, with boundary conditions 21 and 22, has the following analytical solution [16]

$$\frac{c_{THO}}{K_{H_2O}c_{THO}^{HOT}} = \frac{\exp(vx/D_{H_2O})}{\exp(vL/D_{H_2O})} \qquad (23)$$

The flux of THO (N_{THO}) from the hot to the cold reservoir is given by

$$N_{THO} = \left[-D_{H_2O}\frac{dc_{THO}}{dx} + c_{THO}v \right]_{x=0} \qquad (24)$$

When Equations 23 and 24 are combined, the following expression for the water flux is obtained

$$N_{THO} = -\frac{\exp(vL/D_{H_2O})}{1 - \exp(vL/D_{H_2O})} K_{H_2O}(c_{THO}^{HOT})v \qquad (25)$$

This equation was used to generate the curves in Fig. 8 and to compute the fluid velocity v, since the wet membrane thickness (L), the experimentally measured water diffusion and partition coefficients (D_{H_2O} and K_{H_2O}, respectively), the concentration of tritiated water in the hot reservoir (c_{THO}^{HOT}), and the tritiated water molar flux (N_{THO}) are known.

The flow of current across the membrane is related to the movement of charge carriers ($i = F\Sigma z_j N_j$). The

Table 4. Diffusion coefficient of water, bisulphate ion, and proton in 1.0 M H_2SO_4 for the different RAI membrane samples and at infinite dilution. The results reported in [17] for the Nafion and Dow membranes are included

Membrane	$10^6 D_{H_2O}$ /$cm^2 s^{-1}$	$10^6 D_{HSO_4^-}$ /$cm s^{-1}$	$10^6 D_{H^+}$ /$cm^2 s^{-1}$
R-1010	0.680	1.300	2.412
R-4010	3.582	0.531	1.218
R-5010M	0.568	0.200	1.585
Nafion 117	8.800	1.700	14.00
Dow 7-mil	8.100	2.400	20.00
Dow 4-mil	6.900	2.000	15.00
Dow 2.5-mil	6.000	1.800	10.00
infinite dilution [23]	–	13.30	92

flux of ionic species is represented by the following equation

$$N_j = -z_j u_j F c_j \nabla\Phi - D_j \nabla c_j + c_j v \quad (26)$$

Equation 26 can be inverted and combined with the current density equation to obtain the following equation for the electric potential gradient in the membrane

$$\nabla\Phi = \frac{i}{\kappa} - \frac{F}{\kappa}\sum_j z_j D_j \nabla c_j + \frac{F}{\kappa} v \sum_j z_j c_j \quad (27)$$

where κ is the electrical conductivity of the pore electrolyte

$$\kappa = \frac{F^2}{RT}\sum_j z_j^2 D_j c_j$$

No significant concentration gradients of non-radiotracer protons and bisulphate ions existed during our electrodialysis experiments; the second term on the right hand side of Equation 27 can be neglected. When $\nabla\Phi$ is approximated by $\Delta\Phi/L$, the following potential equation is obtained

$$\frac{\Delta\Phi}{L} = -\frac{RT}{F^2}\frac{i}{(c_m D_{H^+}) + (K_{H_2SO_4} c_{H_2SO_4})(D_{H^+} + D_{HSO_4^-})} + \frac{RT}{F}\frac{(c_{H^+}) - (K_{H_2SO_4} c_{H_2SO_4})}{(c_m D_{H^+}) + (K_{H_2SO_4} c_{H_2SO_4})(D_{H^+} + D_{HSO_4^-})} v \quad (28)$$

where R is the universal gas constant and T is the absolute temperature. The concentration of fixed charge sites (c_m) in the membrane is computed from the known membrane dry density (ρ_{dry}), porosity (θ), and ion-exchange capacity (IEC)

$$c_m = \frac{\rho_{dry}(1 - \theta) IEC}{1000} \quad (29)$$

When the potential difference across an ion-exchange membrane is known for a given applied current, Equations 28 and 29 can be used to compute the proton diffusion coefficient (D_{H^+}). Calculated proton diffusion coefficients for the three RAI membranes in 1.0 M H_2SO_4 are listed in Table 4. As previously discussed, the higher degree of cross-linking of the RAI membranes results in smaller proton diffusion coefficients relative to those for the Nafion and Dow membranes.

The transference number (t_j) is the fraction of the current carried by the jth ionic species. From the dilute solution theory, the transference number of the proton species is related to $D_{HSO_4^-}$ and D_{H^+} by

$$t_+ = \frac{z_+^2 D_+ c_+}{(z_-^2 D_- c_- + z_+^2 D_+ c_+)} \quad (30)$$

For brevity, the negative sign has been used to indicate the bisulphate ion, and the positive sign to indicate protons. Computed proton transference number are listed in Table 5. The proton transference number is highest in the R-5010M membrane which is consistent with a low bisulphate ion partition coefficient and lowest bisulphate ion diffusion coefficient.

Table 5. Membrane electrokinetic permeability, equivalent pore diameter, proton transference number, and pore-wall charge density for the different membrane samples in 1.0 M H_2SO_4. See [17] for Nafion and Dow data.

Membrane	$\kappa_\Phi \times 10^{16}$ /cm^2	δ /nm	t_+	$\sigma \times 10^5$ /C cm^{-2}
R-1010	1.79	2.1	0.950	6.85
R-4010	2.44	2.2	0.940	9.05
R-5010M	0.283	1.0	0.991	3.55
Nafion 117	11.3	5.5	0.990	5.65
Dow 7-mil	10.0	4.4	0.991	–
Dow 4-mil	11.0	4.5	0.991	–
Dow 2.5-mil	9.40	4.1	0.990	

The membrane electrokinetic permeability (k_Φ) and an equivalent membrane pore diameter (δ) were determined from the computed velocity of the fluid across the pore. The fluid velocity (v) is expressed by a modified form of Schlögl's equation of motion [15, 19, 21, 27, 28]

$$v = \frac{k_\Phi}{\mu} z_m c_m F \nabla\Phi \quad (31)$$

where μ is the fluid viscosity, c_m is the concentration of fixed-charge sites in the membrane, $\nabla\Phi$ is the electric potential gradient, and k_Φ is the electrokinetic permeability. (Pressure gradients are not important in this study, as no enforced pressure difference were employed.) The specific surface of the membrane exposed to fluid (S_0) is related to the electrokinetic permeability and the membrane porosity (θ) by the Kozeny-Carman relationship [16, 29]

$$S_0^2 = \frac{\theta^3}{5k_\Phi(1 - \theta)^2} \quad (32)$$

For a porous medium composed of cylindrical capillaries, the equivalent pore diameter (δ) is dependent on both S_0 and θ by [29]

$$\delta = \frac{4\theta}{S_0(1 - \theta)} \quad (33)$$

Membrane electrokinetic permeabilities equivalent pore diameters were computed by combining Equations 28 and 31 to 33 with experimental i–$\nabla\Phi$ data. Assuming a cylindrical, parallel pore structure for the RAI membranes, the pore-wall fixed-charge concentration is given by [15]

$$\sigma = \frac{\rho_{dry}(1 - \theta)F)(\delta/2.0)}{2\theta\left(\frac{1000}{IEC}\right)} \quad (34)$$

The results of these calculations are listed in Table 5 and can be used to evaluate membrane performance. The R-5010M membrane was found to have the smallest equivalent pore diameter and pore-wall fixed-charge concentration. This membrane also has the smallest electrokinetic permeability, lowest bisulphate diffusivity (*cf.* Table 4) and the highest counterion transference number. These results suggest that the combined effects of pore-wall charge distribution and pore size regulates electrostatic interactions which

repel coions and attract counterions. Although R-1010 and R-5010M are reported by RAI [18] to have the same ion-exchange capacity (meq g^{-1} dry membrane) their computed pore wall fixed-charge densities differ due to the size and number of pores per unit cross-sectional area of membrane. For straight cylindrical pores, the number of pores per unit area can be computed from the porosity and the cross-sectional area of a single pore:

$$\frac{\text{number of pores}}{\text{cm}^2 \text{ of membrane}} = \frac{\theta}{\text{pore area}} \qquad (35)$$

From this equation, the number of pores per cm^2 for R-1010 and R-5010M are 9.684×10^{12} and 2.672×10^{13}, respectively. Hence, R-5010M has a smaller pore radius, but a larger number of pores per cm^2 of membrane, resulting in a larger total pore wall area over which the fixed charges are distributed. Membrane R-1010 has a lower concentration of pore-wall fixed charges and does not exclude coions as effectively as R-4010, as indicated by the higher partition coefficient and bisulphate ion diffusion coefficient for R-1010 (*cf.* Tables 3 and 4, respectively). The smaller pore diameter for R-1010 as compared to R-4010, however, results in a smaller electrokinetic permeability. As a rough approximation, it can be inferred from these results that for a given membrane porosity, the pore size regulates electrokinetic permeability, while the combined effects of pore size and pore-wall charge density controls coion absorption and diffusivity.

4. Conclusions

Experimental radiotracer and membrane-polarization data were used to determine absorption and transport parameters for water, bisulphate ions, and protons in some promising fuel-cell membranes made from radiation-grafted copolymers.

Two membrane samples had a fluorocarbon polymer matrix (R-1010 and R-4010); the third membrane had a hydrocarbon polymer matrix (R-5010M). Both fluorocarbon membranes had a higher effective porosity and were more conductive than the hydrocarbon-matrix membrane. All three membranes had transport properties similar to those reported for Nafion and the Dow membranes. Membrane sample R-5010M had the smallest pore diameter, which resulted in the highest coion exclusion, lowest water permeability and highest proton transference number of the three RAI membranes. The results indicate that the unusually small electrokinetic permeability is determined by the correspondingly small diameter pores in the R-5010M membrane. The high pore-wall fixed-charge density and narrow pores of the R-5010M membrane increase electrostatic repulsion of coions, yielding a highly selective cation-exchange membrane.

When exposed to an oxidizing medium (10 and 30% H_2O_2), the conductivity of the three RAI samples decreased. In the milder oxidizing environment, however, the R-1010 membrane conductivity decreased by only 15% as compared to an order-of-magnitude decrease for the other two samples. The propensity of the R-4010 and R-5010M membranes to degrade in an oxidizing environment diminished their potential for use in fuel cells. The thinnest fluorocarbon membrane (R-1010) provided facile proton transport while maintaining water permeabilities lower than those exhibited by the Dow and Nafion membranes, which is a desirable characteristic for fuel-cell applications. Also, the sheet resistance of R-1010 was lower than that of the Dow and Nafion membranes. Thus, the use of this RAI membrane would reduce ohmic losses during fuel cell operation. These factors along with its low cost make the R-1010 membrane a promising candidate for fuel-cell applications.

References

[1] F. Sissine, Fuel Cells for Electric Power Production: Future Potential, Federal Role, and Policy Options, in 'FUEL CELLS Trends in Research and Application,' (edited by A. J. Appleby), Hemisphere, New York (1987) pp. 1–18.
[2] A. P. Fickett, *Sci. Am.* **70** (December 1978).
[3] L. J. Nuttal and J. F. McElroy, *J. Soc. Automotive Engineers* (1983) pp. 1–7
[4] R. A. Lemons, *J. Power Sources* **29** (1990) 252–66.
[5] H. G. Wilson, P. B. MacCready and C. R. Kyle, *Sci. Am.* (March 1989) 90–7.
[6] *Fuel Cell News* **V** (edited by M. Gustein) (4) (December 1988).
[7] A. K. Shukla, K. V. Ramesh and A. M. Kannan, *Proc. Indian Acad. Sci. (Chem. Sci.)* **97** (3 and 4) (1986) 513–28.
[8] J. P. Hoare, 'The Electrochemistry of Oxygen,' J. Wiley & Sons (Interscience), New York (1968) 307.
[9] D. M. Bernardi, *J. Electrochem. Soc.* **137** (1990) 3344–50.
[10] K. Kishida, "Status and Interest of Japanese Industrial Development of Fuel Cells", in FUEL CELLS Trends in Research and Application, *op. cit.* [1] (1987) 173–90.
[11] P. C. Rieke and N. E. Vanderborgh, *J. Electrochem. Soc.* **134** (1987) 1099–104.
[12] E. A. Ticianelli, C. R. Derouin and S. Srinivasan, *J. Electroanal. Chem.* **251** (1988) 275.
[13] E. A. Ticianelli, C. R. Derouin, A. Redondo and S. Srinivasan, *J. Electrochem. Soc.* **135** (1988) 2209–14.
[14] P. Savage, *Chemical Week* (March 1987) p. 13.
[15] M. W. Verbrugge and R. F. Hill, *J. Phys. Chem.* **92** (1988) 6778.
[16] M. W. Verbrugge and R. F. Hill, *J. Electrochem. Soc.* **137** (1990) 1131–8.
[17] M. W. Verbrugge and R. F. Hill, *J. Electrochem. Soc.* **137** (1990) 3770–7.
[18] RAIPORE Product and Data Guide, RAI Research Corporation, Long Island, New York (1988).
[19] R. Helfferich, 'Ion Exchange,' McGraw-Hill, New York (1962).
[20] A. Chapiro, 'Radiation Chemistry of Polymeric Systems,' Vol XV of 'High Polymers', J. Wiley & Sons (Interscience), New York (1962).
[21] M. W. Verbrugge, and R. F. Hill, *J. Electrochem. Soc.* **137** (1990) 886.
[22] J. Jensen, 'Materials Research for Advanced Solid-State Fuel Cells of the Energy Research Laboratory, Denmark,' in 'FUEL CELLS Trends in Research and Application', op. cit. [1] (1987) 145–60.
[23] J. Newman, 'Electrochemical Systems,' Prentice-Hall, Englewood Cliffs NJ (1973).
[24] S. W. Capeci, P. N. Pintauro and D. N. Bennion, *J. Electrochem. Soc.* **136** (1989) 2876.
[25] P. N. Pintauro and D. N. Bennion, *I&EC Fundamentals* **23** (1984) 234.
[26] R. B. Bird, W. E. Stewart and E. N. Lightfoot, 'Transport Phenomena,' J. Wiley & Sons, New York (1960).
[27] N. Lakshminarayanaiah, 'Transport Phenomena in Membranes,' Academic Press, London (1969).
[28] R. Schlögl, *Ber. Bunsenges.* **70** (1966) 400–14.
[29] A. E. Scheidegger, 'The Physics of Flow Through Porous Media,' 3rd ed., University of Toronto Press, Toronto (1974) pp. 141–66.